Study on the Photoresponse of Amorphous In−Ga−Zn−O and Zinc Oxynitride Semiconductor Devices by the Extraction of Sub-Gap-State Distribution and Device Simulation

Jun Tae Jang,[†] Jozeph Park,[‡] Byung Du Ahn,[§] Dong Myong Kim,[†] Sung-Jin Choi,[†] Hyun-Suk Kim,*,[#] and Dae Hwan Kim*,[†]

[†]School of Electrical Engineering, Kookmin University, Seoul 136-702, Republic of Korea

[‡]Department of Materials Science and Engineering, KAIST, Daejeon 305-338, Republic of Korea

[§]School of Electrical and Electronic Engineering, Yonsei University, Seoul 120-749, Republic of Korea

[#]Department of Materials Science and Engineering, Chungnam National University, Daejeon 305-764, Republic of Korea

ABSTRACT: Persistent photoconduction (PPC) is a phenomenon that limits the application of oxide semiconductor thin-film transistors (TFTs) in optical sensor-embedded displays. In the present work, a study on zinc oxynitride (ZnON) semiconductor TFTs based on the combination of experimental results and device simulation is presented. Devices incorporating ZnON semiconductors exhibit negligible PPC effects compared with amorphous In−Ga−Zn-O (a-IGZO) TFTs, and the difference between the two types of materials are examined by monochromatic photonic C−V spectroscopy (MPCVS). The latter method allows the estimation of the density of subgap states in the semiconductor, which may account for the different behavior of ZnON and IGZO materials with respect to illumination and the associated PPC. In the case of a-IGZO TFTs, the oxygen flow rate during the sputter deposition of a-IGZO is found to influence the amount of PPC. Small oxygen flow rates result in pronounced PPC, and large densities of valence band tail (VBT) states are observed in the corresponding devices. This implies a dependence of PPC on the amount of oxygen vacancies (V_O). On the other hand, ZnON has a smaller bandgap than a-IGZO and contains a smaller density of VBT states over the entire range of its bandgap energy. Here, the concept of activation energy window (AEW) is introduced to explain the occurrence of PPC effects by photoinduced electron doping, which is likely to be associated with the formation of peroxides in the semiconductor. The analytical methodology presented in this report accounts well for the reduction of PPC in ZnON TFTs, and provides a quantitative tool for the systematic development of phototransistors for optical sensor-embedded interactive displays.

KEYWORDS: persistent photoconductivity, oxide semiconductor, thin-film transistors, In−Ga−Zn-O, zinc oxynitride, density-of-states, phototransistors, sensor-embedded interactive display
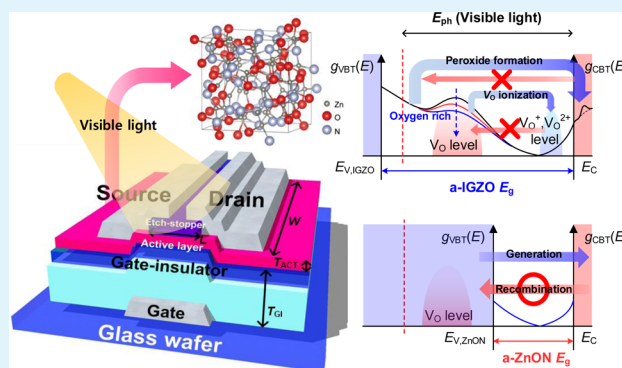
■ INTRODUCTION

The recent development of high-resolution and large size flat panel displays has driven considerable progress in the field of amorphous oxide semiconductors (AOSs), as thin film transistor (TFT) arrays incorporating such materials with high carrier mobility act as fast switching or driving elements in active matrix liquid crystal display (AMLCD) or active matrix organic light emitting diode (AMOLED) panels.[1−4] Although devices based on conventional hydrogenated amorphous silicon (a-Si:H) exhibit relatively low field-effect mobility (<1 cm^2 V^{-1} s^{-1}), TFTs incorporating oxide semiconductors such as amorphous In−Ga−Zn−O (a-IGZO) exhibit high mobility exceeding 5 cm^2 V^{-1} s^{-1} in commercially available products.[5,6]

A potential application of large area flat panels involves the realization of interactive information displays, which allow the users to input information into the hardware, for example, in the form of light signals.[7−9] In this regard, the integration of photosensors is necessary in order to have the hardware detect and process the incoming signals. The incorporation of light sensitive TFT devices is the most straightforward way to implement photodetectors in display backplanes. The use of semiconductors that react to photon radiation is therefore mandatory, and high mobility oxide semiconductors indeed meet such requirements, providing considerable photocurrent in the off region.[9]

However, oxide semiconductor devices exhibit a typical phenomenon known as persistent photoconduction (PPC), which is detrimental regarding their stability under illumina-

tion.[7,10−14] Exposure to light results in the formation of electron−hole pairs, which do not recombine spontaneously when the light is turned off. The excess carrier lifetime may last as long as several days, which induces undesired electrical conductivity in oxide semiconductors even in the absence of light, hence the name PPC. Because of such effects, the threshold voltage of oxide semiconductor TFTs shifts in the negative direction upon prolonged operation, compromising the product reliability.

An alternative semiconductor of choice that exhibits fast recovery after illumination is zinc oxynitride (ZnON), a material with a small bandgap (∼1.3 eV) that usually exhibits relatively high electron mobility (>30 cm^2 V^{-1} s^{-1}).[12,15−17] While providing relatively large photoresponsivity in the off region, once the light is turned off, TFTs based on ZnON recover the initial dark off current levels and threshold voltage immediately. The present work involves the study of the sub-bandgap state distributions in a-IGZO and ZnON semi-conductors based on monochromatic photonic $C-V$ spectros-copy (MPCVS) and device simulation. Sputter-deposited IGZO films using different oxygen flow rates are analyzed first, and the distribution of valence band tail (VBT) states in the bandgap is found to be related with the amount of PPC effect in the corresponding devices. The concept of VBT states cannot be directly compared between a-IGZO and ZnON, as the bandgap of ZnON is smaller than that of a-IGZO (∼3.3 eV). Nevertheless, the density of subgap states over the entire range of the ZnON bandgap is smaller than that in IGZO films. It is suggested that the absence of oxygen-related VBT states in ZnON results in fast electron−hole recombination, resulting in negligible PPC. The concept of activation energy window (AEW) is introduced to explain the occurrence of PPC effects by photoinduced electron doping, which is likely to be associated with the formation of peroxides in the semi-conductor. The analytical methodology presented herein explains well the reduction of PPC in ZnON TFTs, and provides a quantitative tool for the systematic development of photonic devices or optical sensor-embedded interactive displays.

■ EXPERIMENTAL SECTION

Device Fabrication. All samples were prepared on glass substrates. Prior to device fabrication, the substrates were chemically cleaned using aqueous mixtures of $H_2SO_4-H_2O_2$, followed by deionized water rinsing. Bottom-gate and top-contact TFTs were fabricated using standard semiconductor fabrication process as shown in Figure 1.

First, 200 nm-thick molybdenum (Mo) was sputtered at room temperature on the substrate and patterned photolithographically to form the gate electrodes. Then, a stack of silicon nitride (SiN$_x$) and silicon dioxide (SiO$_x$) films was deposited sequentially at 350 °C by plasma-enhanced chemical vapor deposition (PECVD) to form the
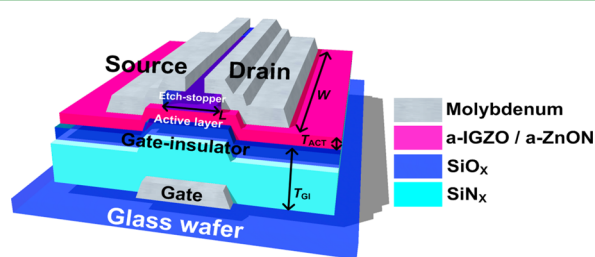
Figure 1. Schematic diagram of the thin film transistor devices fabricated in the present work.

gate insulator. Two different types of semiconductors were employed next. For a-IGZO active layers, 50 nm-thick IGZO thin films were grown at room temperature by direct current (DC) magnetron sputtering using a single In$_2$Ga$_2$ZnO$_7$ target. The deposition was done with various gas mixing ratios of Ar/O$_2$ = 35/20, 35/40, 35/60 sccm at a fixed total pressure of 5 mTorr. On the other hand, for ZnON active layers, thin films of ZnON (50 nm thick) were deposited at room temperature by reactive radio frequency (RF) magnetron sputtering. A Zn metal target was used, and the deposition was done using a gas flow rate ratio of Ar/O$_2$/N$_2$ = 5/1/100 sccm. The active islands were patterned by a wet etch process. Subsequently, a 100 nm thick SiO$_x$ etch stopper layer was deposited at 200 °C by PECVD. After patterning the etch stopper by dry etching, 200 nm thick Mo was sputtered at room temperature and patterned to form the source-drain electrodes. Finally, a 100 nm-thick SiO$_x$/100 nm thick SiN$_x$ bilayer was deposited as the passivation layer. The fabricated devices were annealed in air for 1 h at 250 °C.

Electrical Characterization and Device Simulation. Devices with channel width/length = 50/30 μm were characterized at room temperature. All electrical properties were measured using an Agilent 4156C precision semiconductor parameter analyzer, and the threshold voltage (V_T), subthreshold swing (SS), and the field-effect mobility ($μ_{FE}$) were extracted in compliance with the gradual channel approximation.[18] The V_T was defined as the gate voltage that induces a drain current of 10 nA. The photoresponse of the drain current (I_{DS}) was observed using a halogen lamp with a luminance of 112,000 lx as the light source. The variation of I_{DS} was observed as a function of time while switching the lamp on and off. The subgap density of states (DOS) profiles were extracted from the capacitance−voltage ($C-V$) characteristics of the TFTs. The density distribution of acceptor-like subgap states, $g_A(E)$, and that of donor-like subgap states, $g_D(E)$, were extracted by using the frequency-dependence of $C-V$ and the photonic response of $C-V$ characteristics, respectively. For the latter, a monochromatic light with 532 nm wavelength was used. The current−voltage ($I-V$) characteristics were calculated by combining the extracted DOS and a subgap DOS-based device simulator (DeAOTS). The peroxide electron doping concentration, N_D, was extracted by fitting the measured $I-V$ curves with the calculated ones over a broad range of V_{GS} and V_{DS}.

■ RESULTS AND DISCUSSION

The transfer characteristics of the IGZO and ZnON devices are shown in Figure 2a, b representing the drain-to-source current (I_{DS}) as a function of gate-to-source voltage (V_{GS}) by a linear and a logarithmic scale, respectively. Figure 2c shows the output characteristics of the devices indicating good saturation at large VDS values, and Figure 2d illustrates a comparison of the field effect mobility values of the TFTs in both linear and saturation regimes.

Note the superior field-effect mobility for the ZnON device, whereas in the case of a-IGZO devices, the field-effect mobility decreases with an increase in oxygen gas flow rate used during the sputter deposition. It is suggested that the concentration of oxygen vacancies (V$_O$) decreases with increased oxygen flow rate, resulting in fewer free carrier electrons in IGZO.[19−22] Also, the threshold voltage becomes more positive as the amount of oxygen incorporation becomes larger. The representative electrical parameters reflecting the device performance, including saturation field-effect mobility, thresh-old voltage, and subthreshold swing (SS), are listed in Table 1.

A schematic diagram illustrating the types of subgap states is shown in Figure 3, where E_C denotes the conduction band minimum and E$_V$ is the valence band maximum. In the present work, the distribution of conduction band tail (CBT) states, $g_{CBT}(E)$, and that of valence band tail (VBT) states, $g_{VBT}(E)$, are considered for the interpretation of the device behavior with respect to illumination. For n-type semiconductors, the Fermi
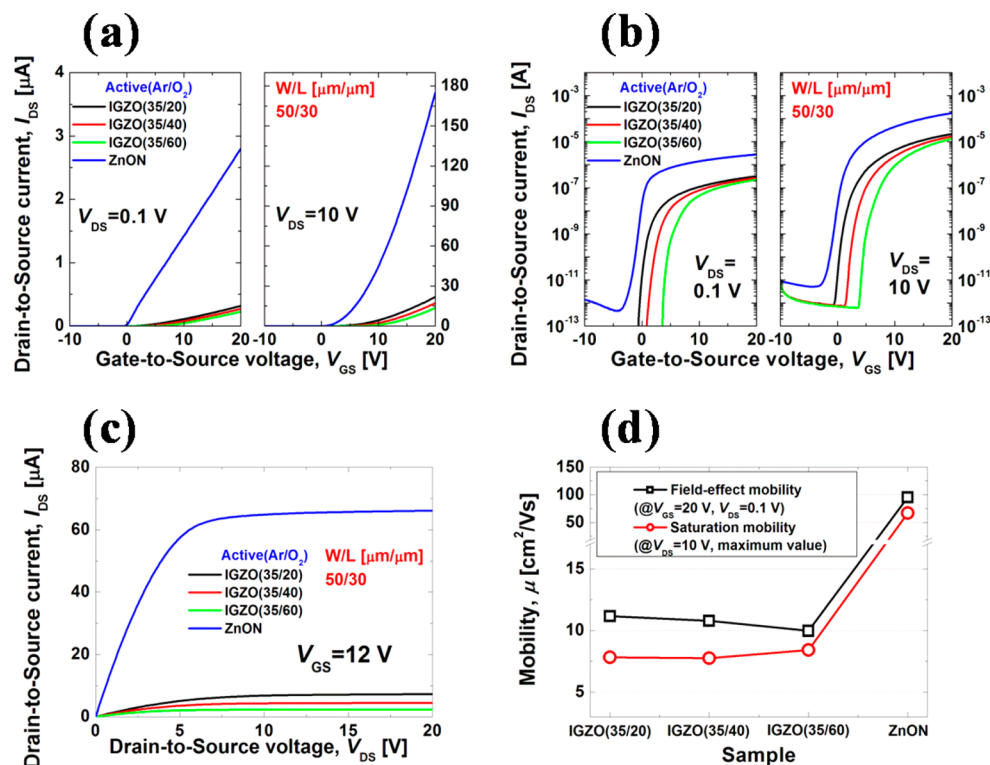
Figure 2. Transfer characteristics of the a-IGZO and ZnON TFT devices represented by a (a) linear and (b) logarithmic scale for I_{DS}. (c) Output curves collected at a fixed V_{GS} = 12 V. (d) Field-effect mobility values of the different devices.

Table 1. Electrical Parameters Extracted from the a-IGZO and ZnON TFT Devices

params	a-IGZO			ZnON
$Ar/O_2/N_2$	35/20/0	35/40/0	35/60/0	5/1/100
$\mu_{FE,SAT}$ (cm^2/(V s))	7.83	7.75	8.42	67.0
V_T @ I_{DS} = 10 nA (V)	2.89	4.73	7.19	−0.19
SS (mV/dec)	627	697	712	555
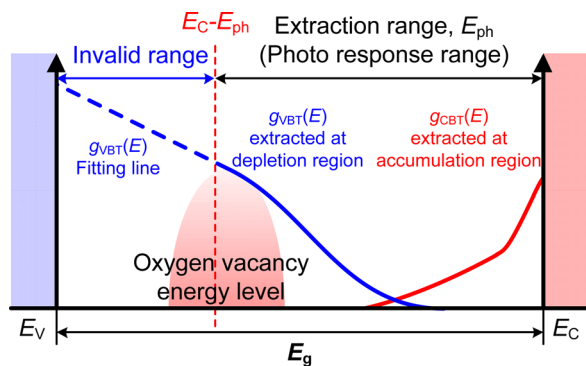
Figure 3. Schematic diagram of the sub-bandgap states, which may be distinguished as valence band tail (VBT) states and conduction band tail (CBT) states. Only the region that can be probed by the incident photon energy may be extracted, and the distribution of VBT states below is simply extrapolated.

energy level lies in the $g_{CBT}(E)$ region during carrier accumulation in the channel, and lies in the $g_{VBT}(E)$ region while the channel is depleted. The CBT states consist of acceptor-like tail states (g_{TA}) and acceptor-like deep states (g_{DA}), whereas the VBT states include donor-like tail states (g_{TD}) and donor-like deep states (g_{DD}). It is well-known in the

field of oxide semiconductors that the donor-like tail states arise from the amorphous structure, whereas part of the donor-like deep states originate from the presence of oxygen vacancies (V_O).[21−23]

The conduction band tail states play an important role in determining the electrical performance of the devices, whereas the valence band tail states influence the stability with respect to bias stress or PPC.[24,25] It is therefore important to understand how the distribution of subgap states affects the a-IGZO and ZnON TFTs regarding their performance and stability. As reported in earlier publications, monochromatic photonic $C−V$ spectroscopy (MPCVS) was performed in order to use the $C−V$ properties measured in the dark and under photon radiation to extract the subgap states density distributions.[26] The symbols in Figure 4a represent the experimentally assessed density of subgap states in the energy range from the conduction band minimum down to the energy provided by the incident photons (532 nm wavelength). The profiles of the states below the deepest level accessible are extrapolated logarithmically, represented by dashed lines.

Figure 4b shows the conduction band tail (CBT) states on a linear scale for all devices. The extracted subgap distributions were modeled and plotted as shown in Figure 4c, using the following equations:

$$g_{CBT}(E) = g_{DA}(E) + g_{TA}(E)$$

$$= N_{DA}\exp\left(\frac{E - E_C}{kT_{DA}}\right) + N_{TA}\exp\left(\frac{E - E_c}{kT_{TA}}\right)$$

$$(cm^{-3}\ eV^{-1}) \tag{1}$$
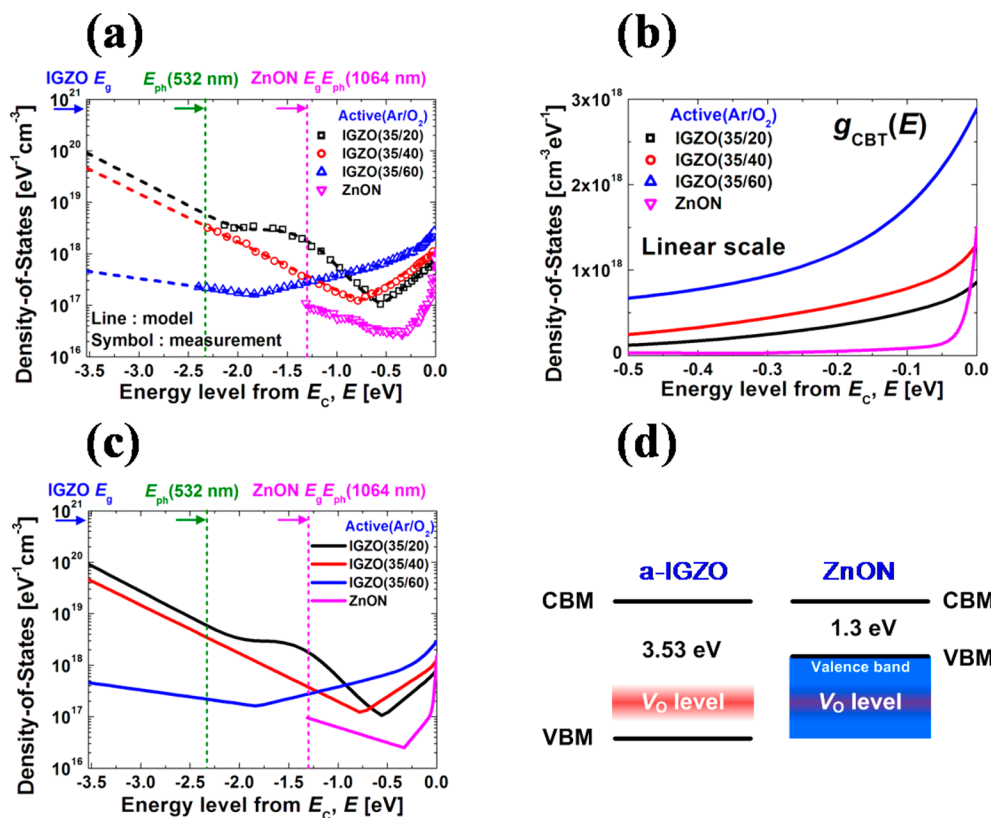
Figure 4. (a) Experimentally extracted density of subgap states for all devices and (b) conduction band tail states near the conduction band minimum represented by a linear scale. (c) Modeled distributions of subgap states using exponential and Gaussian distributions. (d) Schematic illustrating the V_O-related defects in a-IGZO and their negligible effects in ZnON semiconductors.

**Table 2. Parameters Used for the Modeling of Sub-Gap State Density Profiles**

params		a-IGZO			ZnON
$Ar/O_2/N_2$		35/20/0	35/40/0	35/60/0	5/1/100
$g_{CBT}(E)$ $(cm^{-3}\,eV^{-1})$	N_{TA} $(cm^{-3}eV^{-1})$	1.35×10^{17}	2.70×10^{18}	1.79×10^{18}	1.36×10^{18}
	kT_{TA} (eV)	0.026	0.027	0.115	0.013
	N_{DA} $(cm^{-3}eV^{-1})$	7.24×10^{17}	1.04×10^{18}	1.10×10^{18}	1.43×10^{18}
	kT_{DA} (eV)	0.277	0.347	0.942	0.189
$g_{VBT}(E)$ $(cm^{-3}eV^{-1})$	N_{TD} $(cm^{-3}\,eV^{-1})$	9.20×10^{19}	4.63×10^{19}	4.59×10^{17}	9.39×10^{16}
	kT_{TD} (eV)	0.435	0.463	1.622	0.732
	N_{DD} $(cm^{-3}eV^{-1})$	1.77×10^{18}			
	E_{DD} (eV)	1.98			
	kT_{DD} (eV)	0.418			

$$g_{VBT}(E) = g_{DD}(E) + g_{TD}(E)$$

$$= N_{DD} \times \exp\left[-\left(\frac{E_{DD} - E}{kT_{DD}}\right)^2\right]$$

$$+ N_{TD} \times \exp\left(\frac{E_V - E}{kT_{TD}}\right) [cm^{-3}\,eV^{-1}] \quad (2)$$

The parameters used to fit the subgap distributions are listed in Table 2.

The extracted DOS distributions clearly vary with the amount of oxygen incorporated during the sputter growth of IGZO semiconductors. For oxygen-deficient IGZO ($Ar/O_2 = 35/20$ sccm), a Gaussian peak is observed, centered at $E = E_V + 1.98$ eV. This peak is not present when the oxygen content in IGZO is increased ($Ar/O_2 = 35/40$ and $35/60$ sccm). It is

highly likely that this peak is related with the presence of oxygen vacancies. Former reports available in the literature estimated the position of the V_O energy level at approximately $1-1.5$ eV above E_V;[23,27] however, the latter resulted from theoretical calculations, and the position observed in the present work may differ by approximately 0.5 eV. Although the exact position of the V_O peak may vary according to the properties of the deposited IGZO material, this is the first V_O peak reported up to date observed by experimental extraction of subgap states. The conduction band tail (CBT) states decrease with increased V_O content in a-IGZO, whereas the valence band tail (VBT) states exhibit the opposite trend. On the other hand, the VBT concentration in ZnON near its E_V is considerably smaller than those of IGZO devices. It was previously reported by ab initio calculations that the states related to V_O are located below the valence band minimum of N-rich ZnON as shown schematically in Figure 4d, and thus
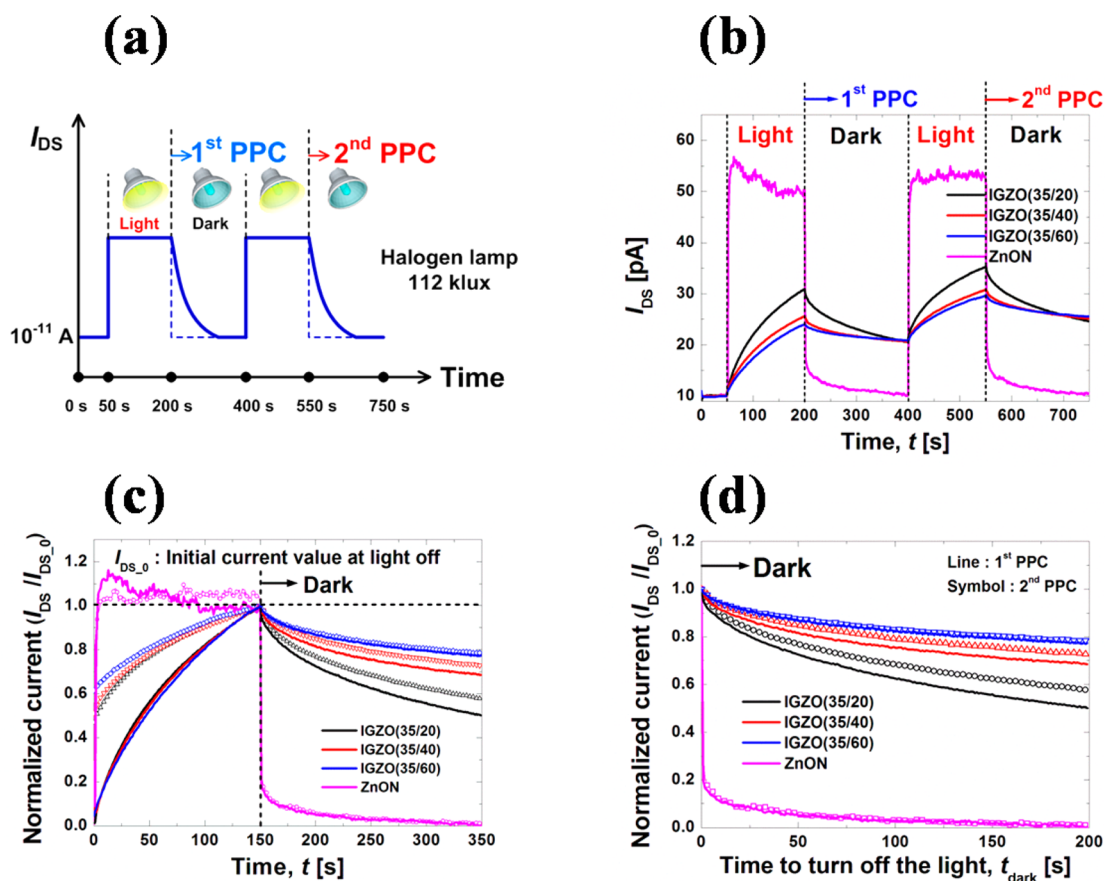
Figure 5. (a) Experimental setup for PPC evaluation. (b) Photocurrent as a function of time for the a-IGZO and ZnON devices, with the light switched on and off. (c) Normalized current levels indicating the recovery behavior after the light is turned off. (d) Normalized current levels immediately after light is turned off, reflecting the fast recovery of ZnON TFT.

PPC effects could be suppressed.[12,16] The next results involve the PPC evaluation of a-IGZO and ZnON devices upon repeated exposure to visible light, and how their response to photon radiation is related to VBT states.

Figure 5a illustrates the experimental setup for PPC evaluation. Each exposure of the TFTs to light was maintained for 150 s and between each exposure the devices were let to recover for 200 s. For each device, the V_{GS} was fixed at the value inducing I_{DS} = 10 pA, and the I_{DS} variations were monitored as a function of time, for two sequential exposures to light. Figure 5b shows the photoresponse of the a-IGZO and ZnON devices. Note the fast increase in photocurrent for ZnON upon light exposure and its steplike decrease upon switching the halogen lamp off. In contrast, the a-IGZO devices exhibit exponential increase and decrease in photocurrent, however do not reach the initial value measured in the dark for several hundred seconds, a situation in which PPC is apparent. The IGZO with smaller oxygen content is more sensitive to illumination, exhibiting a large increase in photocurrent. Also, faster recovery than oxygen-rich IGZO devices is observed when the light is turned off, as indicated by the normalized current levels in Figure 5c, d.

It was formerly reported that defects related to oxygen vacancies may trap hole carriers in ZnO-based materials and prevent the electron−hole recombination after exposure to light.[23,28] However, the results presented in this work suggest that higher concentrations of oxygen vacancies (i.e., low oxygen incorporation such as Ar/O$_2$ = 35/20 sccm) induce faster

photoresponse, generating higher free carriers by the excitation of electron hole pairs, and faster recovery by their recombination upon turning the light off. It is therefore conjectured that the trapping of holes by oxygen vacancy ionization ($V_O + 2h^+ \rightarrow V_O^{2+}$) may not be the mechanism inducing PPC in a-IGZO.

A more plausible theory involves the formation of metastable peroxides upon illumination, which may act as net electron donors ($O^{2-} + O^{2-} + 2h^+ + 2e^- \rightarrow O_2^{2-} + 2e^-$).[29] According to ab initio calculations, the recovery process of the peroxide ($O_2^{2-} + 2e^- \rightarrow O^{2-} + O^{2-}$) is thermodynamically favorable, but an energy barrier makes the recovery rather sluggish, which results in PPC. The reported value of this energy barrier is approximately 0.97 eV, which matches well with the experimentally observed activation energy of 0.9−1.0 eV.[13] It may therefore be understood that the PPC effect originates from the excitation of electron−hole pairs from the valence band tail (VBT) states, and the peroxide model describes well the slow recovery in a-IGZO devices, whereas the VBT-deficient ZnON TFT exhibits negligible PPC. Figure 6 is a schematic diagram illustrating the ionization of oxygen vacancies and the subsequent peroxide formation. Larger V_O concentrations in a-IGZO induce larger $g_{VBT}(E)$, which results in larger densities of ionized vacancies (V_O^{2+}) and peroxides. Also, the larger the number of photoinduced electrons, the larger is the probability of having them recombined with V_O^{2+} or having the peroxides recover the original state ($O_2^{2-} + 2e^- \rightarrow O^{2-} + O^{2-}$). This explains well the relatively fast recovery of
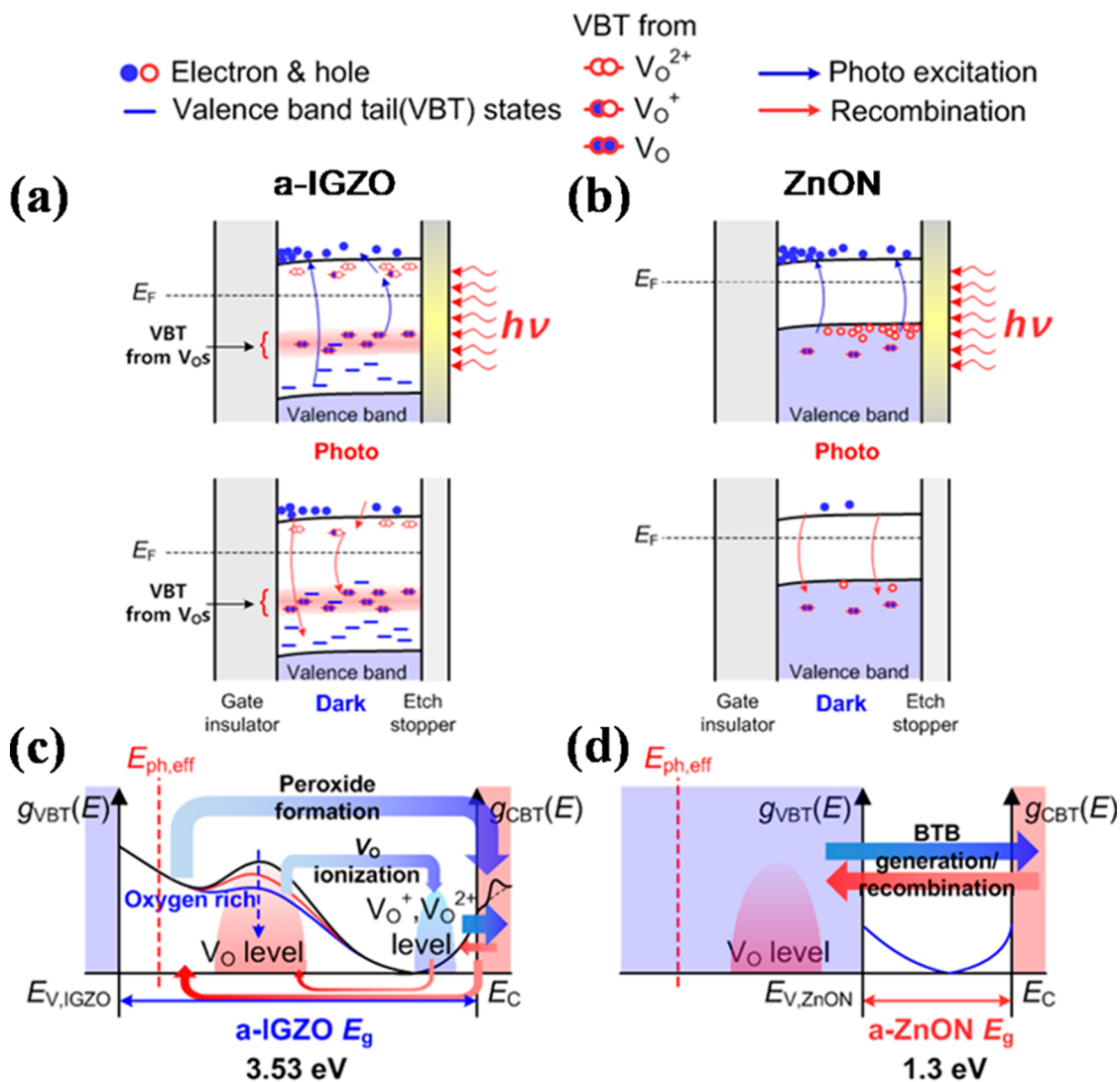
Figure 6. Schematic energy band diagrams illustrating the ionization of oxygen vacancies, the formation of peroxides, and their recovery from PPC by recombination in (a) a-IGZO and (b) ZnON devices. (c) Schematic representation of V_O ionization and peroxide formation from the photoexcitation of sub-bandgap states. (d) Schematic illustration of direct band-to-band generation and recombination in ZnON.
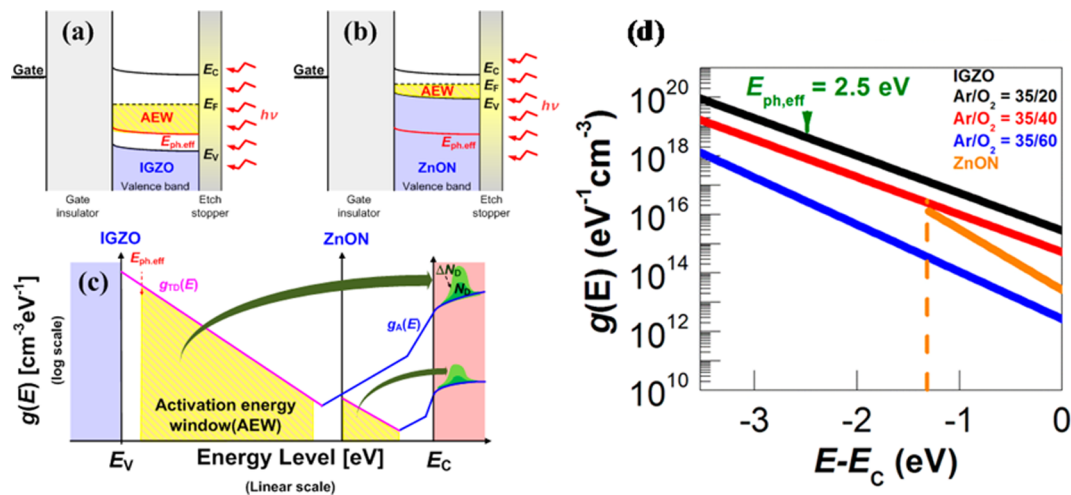
Figure 7. Schematic diagram showing the activation energy window (AEW) in (a) a-IGZO and (b) ZnON. (c) Concept of electron doping by photoexcited VBT states in a-IGZO and ZnON, the shaded area corresponding to the AEW. (d) Quantified AEW for a-IGZO and ZnON devices, based on $g_{VBT}(E)$ curves.

the a-IGZO device with the smallest amount of oxygen incorporated (Ar/O_2 = 35/20 sccm).

In the case of ZnON semiconductors, direct band-to-band generation and recombination of photoexcited carriers are anticipated to take place, owing to the relatively small bandgap ($\sim$1.3 eV). This is highly likely to be the mechanism that governs the fast photoresponse and recovery of the ZnON devices. Here, neither V_O ionization nor peroxide formation takes effect.

To quantify the PPC effect, a concept of activation energy window (AEW) is defined by the following equation[30]

$$AEW(E) = \int_{E_C - E_{ph,eff}}^{E_F} g_{VBT}(E)dE \ (cm^{-3}) \tag{3}$$

The AEW represents the increment in electron doping concentration, ΔN_D, by the photoexcitation of VBT states. It is assumed that a sufficient number of photons are available to excite electron from all states that can be probed by the incident photon energy within the bandgap. Figure 7 is a schematic illustrating the concept of activation energy window, and the quantification of AEW by integrating the area under the VBT curves.

The AEW values are listed in Table 3. The Fermi energy level for each case is determined by the electrical measurement conditions such as V_{GS} and V_{DS}.

Table 3. Activation Energy Window (AEW) for the a-IGZO and ZnON TFTs

params		IGZO		ZnON
$Ar/O_2/N_2$	35/20/0	35/40/0	35/60/0	5/1/100
V_{GS} @ I_{DS} = 10 pA (V)	1.3	3.2	5.5	−0.8
AEW (cm^{-3})	1.11×10^{18}	2.79×10^{17}	7.73×10^{15}	2.67×10^{15}

CONCLUSION

The photoresponse behavior of a-IGZO and ZnON TFTs was investigated by MPCVS extraction of sub-bandgap states and in terms of persistent photoconduction (PPC). Although ZnON devices exhibit superior performance than their a-IGZO counterparts, they also undergo fast excitation and recovery upon exposure to visible light. The PPC effect in a-IGZO is most likely to originate from the formation of peroxides, rather than V_O ionization. Direct band-to-band carrier generation and recombination is anticipated to be the reason for fast photoresponse and recovery in ZnON devices. The number of valence band tail (VBT) states is directly related to the number of photoexcited carriers, which is represented by the activation energy window (AEW). The methodology presented in this work, based on the subgap DOS extraction and device simulation, is demonstrated to be a suitable tool for the design of photosensors with high mobility and negligible PPC. ZnON is an appropriate semiconductor that satisfies the latter criteria, and is applicable to large-area interactive displays.

AUTHOR INFORMATION

Corresponding Authors

*E-mail: khs3297@cnu.ac.kr.
*E-mail: drlife@kookmin.ac.kr .

Author Contributions

J.T.J. and J.P. (jozeph.park@gmail.com) contributed equally to this work. The manuscript was written through contributions of all authors. All authors have given approval to the final version of the manuscript.

Notes

The authors declare no competing financial interest.

ACKNOWLEDGMENTS

REFERENCES

(1) Nomura, K.; Ohta, H.; Takagi, A.; Kamiya, T.; Hirano, M.; Hosono, H. Room-Temperature Fabrication of Transparent Flexible Thin-Film Transistors using Amorphous Oxide Semiconductors. *Nature (London, U. K.)* **2004**, *432*, 488−492.

(2) Park, J. S.; Maeng, W.-J.; Kim, H.-S.; Park, J.-S. Review of Recent Developments in Amorphous Oxide Semiconductor Thin-Film Transistor Devices. *Thin Solid Films* **2012**, *520*, 1679−1693.

(3) Park, J.-S.; Kim, H.; Kim, I.-D. Overview of Electroceramic Materials for Oxide Semiconductor Thin Film Transistors. *J. Electroceram.* **2014**, *32*, 117−140.

(4) Rim, Y. S.; Chen, H.; Kou, X.; Duan, H.-S.; Zhou, H.; Cai, M.; Kim, H. J.; Yang, Y. Boost Up Mobility of Solution-Processed Metal Oxide Thin-Film Transistors via Confining Structure on Electron Pathways. *Adv. Mater.* **2014**, *26*, 4273−4278.

(5) Nam, W.-J.; Shim, J.-S.; Shin, H.-J.; Kim, J.-M.; Ha, W.-S.; Park, K.-H.; Kim, H.-G.; Kim, B.-S.; Oh, C.-H.; Ahn, B.-C.; Kim, B.-C.; Cha, S.-Y. 55-in. OLED TV using InGaZnO TFTs with WRGB Pixel Design. *Dig. Tech. Pap. - Soc. Inf. Disp. Int. Symp.* **2013**, *44*, 243−246.

(6) Chen, C.-Y.; Lin, L.-F.; Lee, J.-Y.; Wu, W.-H.; Wang, S.-C.; Chiang, Y. M.; Chen, Y.-H.; Chen, C.-C.; Chen, Y.-H.; Chen, C.-L.; Shih, T.-H.; Liu, C.-H.; Ting, H.-C.; Lu, H.-H.; Tsai, L.; Lin, H.-S.; Chang, L.-H.; Lin, Y.-H. A 65-in. Amorphous Oxide Thin Film Transistors Active-Matrix Organic Light-Emitting Diode Television Using Side by Side and Fine Metal Mask Technology. *Dig. Tech. Pap. - Soc. Inf. Disp. Int. Symp.* **2013**, *44*, 247−250.

(7) Jeon, S.; Ahn, S.-E.; Song, I.; Kim, C. J.; Chung, U.-I.; Lee, E.; Yoo, I.; Nathan, A.; Lee, S.; Robertson, J.; Kim, K. Gated Three-Terminal Device Architecture to Eliminate Persistent Photoconductivity in Oxide Semiconductor Photosensor Arrays. *Nat. Mater.* **2012**, *11*, 301−305.

(8) Ahn, S.-E.; Song, I.; Jeon, S.; Jeon, Y. W.; Kim, Y.; Kim, C.; Ryu, B.; Lee, J.-H.; Nathan, A.; Lee, S.; Lee, G. T.; Chung, U.-I. Metal Oxide Thin Film Phototransistor for Remote Touch Interactive Displays. *Adv. Mater.* **2012**, *24*, 2631−2636.

(9) Lee, E.; Benayad, A.; Shin, T.; Lee, H.; Ko, D.-S.; Kim, T. S.; Son, K. S.; Ryu, M.; Jeon, S.; Park, G.-S. Nanocrystalline ZnON; High Mobility and Low Band Gap Semiconductor Material for High Performance Switch Transistor and Image Sensor Application. *Sci. Rep.* **2014**, *4*, 4948.

(10) Ghaffarzadeh, K.; Nathan, A.; Robertson, J.; Kim, S.; Jeon, S.; Kim, C.; Chung, U.-I.; Lee, J.-H. Instability in Threshold Voltage and Subthreshold Behavior in Hf-In-Zn-O Thin Film Transistors Induced by Bias-and Light-Stress. *Appl. Phys. Lett.* **2010**, *97*, 113504.

(11) Ghaffarzadeh, K.; Nathan, A.; Robertson, J.; Kim, S.; Jeon, S.; Kim, C.; Chung, U.-I.; Lee, J.-H. Persistent Photoconductivity in Hf-In-Zn-O Thin Film Transistors. *Appl. Phys. Lett.* **2010**, *97*, 143510.

(12) Kim, H.-S.; Jeon, S. H.; Park, J. S.; Kim, T. S.; Son, K. S.; Seon, J.-B.; Seo, S.-J.; Kim, S.-J.; Lee, E.; Chung, J. G.; Lee, H.; Han, S.; Ryu, M.; Lee, S. Y.; Kim, K. Anion Control as a Strategy to Achieve High-

Mobility and High-Stability Oxide Thin-Film Transistors. *Sci. Rep.* **2013**, *3*, 1459.

(13) Lee, D. H.; Kawamura, K.; Nomura, K.; Kamiya, T.; Hosono, H. Large Photoresponse in Amorphous In−Ga−Zn−O and Origin of Reversible and Slow Decay. *Electrochem. Solid-State Lett.* **2010**, *13*, H324−H327.

(14) Lee, D. H.; Kawamura, K.; Nomura, K.; Yanagi, H.; Kamiya, T.; Hirano, M.; Hosono, H. Steady-State Photoconductivity of Amorphous In-Ga-Zn-O. *Thin Solid Films* **2010**, *518*, 3000−3003.

(15) Ok, K.-C.; Jeong, H.-J.; Kim, H.-S.; Park, J.-S. Highly Stable ZnON Thin-Film Transistors With High Field-Effect Mobility Exceeding 50 cm^2/Vs. *IEEE Electron Device Lett.* **2015**, *36*, 38−40.

(16) Ryu, M.; Kim, T. S.; Son, K. S.; Kim, H.-S.; Park, J. S.; Seon, J.-B.; Seo, S.-J.; Kim, S.-J.; Lee, E.; Lee, H.; Jeon, S. H.; Han, S.; Lee, S. Y. High Mobility Zinc Oxynitride-TFT with Operation Stability under Light-Illuminated Bias-Stress Conditions for Large Area and High Resolution Display Applications. *Technol. Dig.—Int. Electron Devices Meet.* **2012**, 112−114.

(17) Kim, T.-S.; Kim, H.-S.; Park, J. S.; Son, K. S.; Kim, E. S.; Seon, J.-B.; Lee, S.; Seo, S.-J.; Jun, S.; Lee, K. M.; Shin, D. J.; Lee, J.; Jo, C.; Choi, S.-J.; Kim, D. M.; Kim, D. H.; Ryu, M.; Choi, S.-H.; Park, Y. High Performance Gallium-Zinc Oxynitride Thin Film Transistors for Next-Generation Display Applications. *Technol. Dig.—Int. Electron Devices Meet.* **2013**, 660−662.

(18) Sze, S. M.; Ng, K. K. *Physics of Semiconductor Devices*; Wiley: New York, 2007.

(19) Kim, Y.-S.; Park, C. H. Rich Variety of Defects in ZnO via an Attractive Interaction between O Vacancies and Zn Interstitials: Origin of n-type Doping. *Phys. Rev. Lett.* **2009**, *102*, 086403.

(20) Janotti, A.; Van de Walle, C. G. Hydrogen Multicenter Bonds. *Nat. Mater.* **2007**, *6*, 44−47.

(21) Janotti, A.; Van de Walle, C. G. Native Point Defects in ZnO. *Phys. Rev. B: Condens. Matter Mater. Phys.* **2007**, *76*, 165202.

(22) Robertson, J. Disorder and Instability Processes in Amorphous Conducting Oxides. *Phys. Status Solidi B* **2008**, *245*, 1026−1032.

(23) Janotti, A.; Van de Walle, C. G. Oxygen Vacancies in ZnO. *Appl. Phys. Lett.* **2005**, *87*, 122102.

(24) Kim, Y.; Bae, M.; Kim, W.; Kong, D.; Jeong, H. K.; Kim, H.; Choi, S.; Kim, D. M.; Kim, D. H. Amorphous InGaZnO Thin-Film Transistors—Part I: Complete Extraction of Density of States over the Full Subband-Gap Energy Range. *IEEE Trans. Electron Devices* **2012**, *59*, 2689−2698.

(25) Kim, Y.; Kim, S.; Kim, W.; Bae, M.; Jeong, H. K.; Kong, D.; Choi, S.; Kim, D. M.; Kim, D. H. Amorphous InGaZnO Thin-Film Transistors—Part II: Modeling and Simulation of Negative Bias Illumination Stress-Induced Instability. *IEEE Trans. Electron Devices* **2012**, *59*, 2699−2706.

(26) Bae, H.; Choi, H.; Jun, S.; Jo, C.; Kim, Y. H.; Hwang, J. S.; Ahn, J.; Oh, S.; Bae, J.-U.; Choi, S.-J.; Kim, D. H.; Kim, D. M. Single-Scan Monochromatic Photonic Capacitance-Voltage Technique for Extraction of Subgap DOS Over the Bandgap in Amorphous Semiconductor TFTs. *IEEE Electron Device Lett.* **2013**, *34*, 1524−1526.

(27) Nathan, A.; Lee, S.; Jeon, S.; Song, I.; Chung, U.-I. Transparent Oxide Semiconductors for Advanced Display Applications. *Dig. Technol. Pap.—Soc. Inf. Dispersion Int. Symp.* **2013**, *29*, 6−11.

(28) Ryu, B.; Noh, H.-K.; Choi, E.-A.; Chang, K. J. O-Vacancy as the Origin of Negative Bias Illumination Stress Instability in Amorphous In-Ga-Zn-O Thin Film Transistors. *Appl. Phys. Lett.* **2010**, *97*, 022108.

(29) Nahm, H.-H.; Kim, Y.-S.; Kim, D. H. Instability of Amorphous Oxide Semiconductors via Carrier-Mediated Structural Transition between Disorder and Peroxide State. *Phys. Status Solidi B* **2012**, *249*, 1277−1281.

(30) Jang, J.; Kim, D. G.; Kim, D. M.; Choi, S.-J.; Lim, J.-H.; Lee, J.-H.; Kim, Y.-S.; Ahn, B. D.; Kim, D. H. Investigation on the Negative Bias Illumination Stress-Induced Instability of Amorphous Indium-Tin-Zinc-Oxide Thin Film Transistors. *Appl. Phys. Lett.* **2014**, *105*, 152108.